Received: 21 May 2020 | Revised: 27 August 2020 | Accepted: 14 September 2020

DOI: 10.1111/jnc.15193

ORIGINAL ARTICLE

Journal of Neurochemistry JNC The Official Journal of the International Society for Neurochemistry WILEY

A nuclear fluorescent dye identifies pericytes at the neurovascular unit

Sandra P. Mai-Morente[1] | Virginia M. Marset[1] | Fabiana Blanco[2] | Eugenia E. Isasi[3] | Verónica Abudara[1]

[1]Departamento de Fisiología, Facultad de Medicina, Universidad de la República, Montevideo, Uruguay

[2]Departamento de Biofísica, Facultad de Medicina, Universidad de la República, Montevideo, Uruguay

[3]Departamento de Histología y Embriología, Facultad de Medicina, Universidad de la República, Montevideo, Uruguay

Correspondence
Verónica Abudara, Departamento de Fisiología, Facultad de Medicina, Universidad de la República, General Flores 2125, Montevideo, CP 11800, Uruguay.
Email: abudara@fmed.edu.uy

FUNDING INFORMATION
This work was supported by the "Comisión Sectorial de Investigación Científica de la Universidad de la República Oriental del Uruguay" (Proyecto de Investigación y Desarrollo CSIC I+D 2014, ID 48 to VA; Proyecto de Iniciación a la Investigación 2017, ID 139 to EEI; and financial support for Full-Time researchers to VA and FB), and by "Agencia Nacional de Investigación e Innovación-ANII-Uruguay" (Proyecto de Investigación Fundamental Fondo Clemente Estable FCE_1_2017_1_136103 to VA, Doctoral Fellowship to SPM and Master Fellowship to VM).

Abstract

Perivascular pericytes are key regulators of the blood–brain barrier, vascular development, and cerebral blood flow. Deciphering pericyte roles in health and disease requires cellular tracking; yet, pericyte identification remains challenging. A previous study reported that the far-red fluorophore TO-PRO-3 (642/661), usually employed as a nuclear dye in fixed tissue, was selectively captured by live pericytes from the subventricular zone. Herein, we validated TO-PRO-3 as a specific pericyte tracer in the nervous system (NS). Living pericytes from ex vivo murine hippocampus, cortex, spinal cord, and retina robustly incorporated TO-PRO-3. Classical pericyte immunomarkers such as chondroitin sulphate proteoglycan neuron-glial antigen 2 (NG2) and platelet-derived growth factor receptor beta antigen (PDGFrβ) and the new pericyte dye NeuroTrace 500/525 confirmed cellular specificity of dye uptake. The TO-PRO-3 signal enabled quantification of pericytes density and morphometry; likewise, TO-PRO-3 labeling allowed visualization of pericytes associated with other components of the neurovascular unit. A subset of TO-PRO-3 stained cells expressed the contractile protein α–SMA, indicative of their ability to control the capillary diameter. Uptake of TO-PRO-3 was independent of connexin/pannexin channels but was highly sensitive to temperature and showed saturation, suggesting that a yet unidentified protein-mediated active transport sustained dye incorporation. We conclude that TO-PRO-3 labeling provides a reliable and simple tool for the bioimaging of pericytes in the murine NS microvasculature.

KEYWORDS
blood–brain barrier, neurovascular unit, pericytes imaging, TO-PRO-3

Abbreviations: ACSF, artificial cerebrospinal fluid; AU, arbitrary units; BBB, blood–brain barrier; BSA, bovine serum albumin; CBX, carbenoxolone; CNS, central nervous system; Cx, connexin; DAPI, 2-[4-(Aminoiminomethyl) phenyl]-1H-Indole-6-carboximidamide hydrochloride; ECs, endothelial cells; FITC, fluorescein isothiocyanate; GFAP, glial fibrillary acidic protein; ISOB4, Isolectin B4; IF, immunofluorescence; IHC, immunohistochemistry; NeuN, neuronal nuclear protein; NG2, chondroitin sulfate proteoglycan neuron-glial antigen 2; NVU, neurovascular unit; Panx1, Pannexin1; PBS, phosphate-buffered saline; PBST, phosphate-buffered saline with Triton; PDGFRβ, platelet-derived growth factor receptor beta; PECAM-1, platelet endothelial cell adhesion molecule; PFA, paraformaldehyde; α–SMA, alpha-smooth muscle actin; TO-PRO-3, quinolinium, 4-[3-(3-methyl-2(3H)-benzothiazolylidene)-1-propenyl]-1-[3-(trimethylammonio) propyl]-, diiodide/ 157199–63–8; VSMCs, vascular smooth muscle cells.

1 | INTRODUCTION

Capillary pericytes are essential constituents of the neurovascular unit (NVU) that play pivotal roles in the maintenance and regulation of the blood–brain barrier (BBB) (Armulik et al., 2010), vascular development (Daneman et al., 2010), and cerebral blood flow. Nonetheless, their relative contribution to hyperemia and neurovascular coupling remains under debate (Attwell et al., 2016; Fernández-Klett et al., 2010; Grutzendler & Nedergaard, 2019; Hall et al., 2014; Hill et al., 2015; Kisler et al., 2017, 2020; Kisler, et al., 2017; Mishra et al., 2016; Nelson et al., 2020; Peppiatt et al., 2006). Loss and dysfunction of contractile pericytes are believed to exacerbate neuropathological conditions associated with impairments of microvasculature and neuronal energy supply such as ischemia (Kisler, et al., 2017; Montagne et al., 2018; Nikolakopoulou et al., 2019; Yemisci et al., 2009) and Alzheimer's disease (Hamilton et al., 2010; Montagne et al., 2015, 2020; Nation et al., 2019; Nortley et al., 2019; Sagare et al., 2013).

Unravelling pericytes´ functions in physiological and pathological conditions requires identification of pericytes; thus far, recognition of these mural cells is still a matter of research. Pericytes are routinely identified based on the expression of their surface antigens, typically the chondroitin sulfate proteoglycan neuron-glial antigen 2 (NG2) and the platelet-derived growth factor receptor beta antigen (PDGFrβ) (Hartmann et al., 2015a, b; Lindahl et al., 1997; Ozerdem et al., 2001; Smyth et al., 2018). Accordingly, transgenic mouse lines commonly used to visualize pericytes are driven by promoters for NG2 and PDGFrβ; these reporter mice allow for fluorescence imaging of cerebral pericytes ex vivo and in vivo (Mishra et al., 2014; Hartmann, et al., 2015a,b; Jung et al., 2018). However, using transgenic lines or immunohistochemistry to track pericytes in studies employing mouse models, becomes expensive and time-consuming. Moreover, PDGFrβ and NG2 antigens are also present in vascular smooth muscle cells (VSMCs) and oligodendrocyte progenitors (He et al., 2016; Nishiyama et al., 2009) and other pericyte molecular markers such as desmin and CD13 are also expressed by vascular cells (Armulik et al., 2010; Jung et al., 2018; Smyth et al., 2018). Then, unambiguous discrimination between pericytes and VSMCs (which is a determinant to assess their relative role in neurovascular coupling) remains a subject of study (Attwell et al., 2016; Fernández-Klett et al., 2010; Grutzendler & Nedergaard, 2019; Hall et al., 2014; Hill et al., 2015; Peppiatt et al., 2006). In the future, identification of genes exclusively expressed by pericapillary pericytes might provide cues to differentiate pericytes from VSMCs (Bondjers et al., 2006; Chasseigneaux et al., 2018; He et al., 2016; Vanlandewijck et al., 2018). Recently, the fluorophore NeuroTrace 500/525, which normally stains neurons in fixed tissue, has been shown to selectively label brain capillary pericytes if administered in vivo; so far NeuroTrace 500/525 does not trace VSMCs (Damisah et al., 2017).

In this scenario, previous work has reported that the fluorophore TO-PRO-3 Iodide (642/661), usually employed as a nuclear stain in fixed sections, labels perivascular pericytes from the post-natal subventricular zone when applied to acute slices (Lacar et al., 2012). The TO-PRO-3 dye is a carbocyanine monomer with higher affinity for DNA than for RNA that has been typically used in fixed preparations for immunofluorescence counter-staining and for measuring relative DNA content (Van Hooijdonk et al., 1994; de Mazière et al., 1996; Suzuki et al., 1997). However, in the living tissue TO-PRO-3 becomes a pericyte marker. Brain slices with TO-PRO-3-stained pericytes of the post-natal subventricular zone have been used for live imaging and immunostaining post-fixation (Lacar et al., 2012). Until now, the latter study is the only publication supporting the role of TO-PRO-3 as a pericyte tracer,but neither its specificity nor its staining properties have been further elucidated.

Herein, we show that living pericytes of the nervous system selectively uptake the fluorescent nuclear tracer TO-PRO-3 allowing their unambiguous identification. We characterized morphometry, abundance, α-SMA-expression, rapports, and mechanisms supporting dye uptake of TO-PRO-3^{+}-pericytes. Based on our findings, we conclude that TO-PRO-3 labeling provides a powerful tool to target capillary pericytes at the neurovascular interface.

2 | MATERIALS AND METHODS

2.1 | Animals

Experimental procedures were conducted following the National Institutes of Health guidelines for the care and use of laboratory animals (NIH Publications No. 8023, revised 1978) and the local regulation [CDC Exp. 4332/99, Diario Oficial No. 25467, Feb. 21/00, Universidad de la República, Uruguay]. The Committee on Animal Research Ethics (Law 18.611) (Facultad de Medicina – Udelar) approved the protocol. The ARRIVE guidelines have been followed. To minimize the number of animals used and their suffering, we tested several conditions in slices derived from the same animal. Mice (*Mus musculus*; P20-P30 unless specified) on a C57BL/6 background and rats (*Sprague–Dawley*; P30) from both sexes were used (57 mice and 6 rats). Mice (RRID: IMSR_JAX:000664) were supplied by the Jackson Laboratory and rats (*SD*, Strain code 400) were acquired from Charles River Laboratories. Animals were bred and housed in a temperature- and humidity-controlled room on a 12-hr light/dark cycle at the Unit of Experimental Reactives and Biomodels (URBE - Facultad de Medicina). All these animals were fed ad libitum with chow diet and water. At the time of assaying, mice and rats weighed respectively 10–13 g and 40–100 g. We conducted most experiments at 11 a.m.–3 p.m. No blinding was performed, neither during experiments nor during analysis. No exclusion criteria were pre-determined; animals were arbitrarily assigned in the study.

2.2 | Reagents and antibodies

The fluorescent markers, Fluoresceinisothiocyanate–dextran 70,000 (FITC-Dextran 70S; FD70S; cat.no. 46945), 2-(4-Amidinophenyl)-6-indolecarbamidine dihydrochloride, 4′,6-Diamidino-2-phenylindole

dihydrochloride, DAPI dihydrochloride (DAPI; cat.no. D09542) and Isolectin B4 conjugated to fluorescein (FITC-ISOB4; cat.no. L2895) were acquired from Sigma-Aldrich. The dyes TO-PRO™-3 Iodide 642/661 (cat.no. T3605) and Neurotrace™ 500/525 Green Fluorescent Nissl (cat.no. N21480) were from ThermoFisher Scientific. The connexin/pannexin blocker carbenoxolone (CBX; cat.no. C4790) was purchased from Sigma-Aldrich; the mimetic peptide against pannexin1 (^{10}Panx1; cat.no. 707231_5) was synthesized by GenScript USA Inc. (Piscataway, NJ 08854, USA). Primary antibodies rabbit polyclonal anti-PDGFrβ (cat.no. ab107169, RRID: AB_11156765), rabbit monoclonal anti-NeuN neuronal marker (cat.no. ab177487, RRID: AB_2532109), and rabbit monoclonal anti-α-SMA (cat.no. ab124964, RRID: AB_11129103) were purchased from Abcam. Mouse monoclonal anti-NG2 (cat.no. MAB5384, RRID: AB_177646) was supplied by Millipore and mouse monoclonal anti-GFAP (cat.no. C9205, RRID: AB_476889) was purchased from Sigma-Aldrich. The mouse monoclonal anti-PECAM-1 (cat.no. 2H8, RRID: AB_2161039) developed by Bogen, S.A. (Pathology & Lab Medicine, Boston University) was obtained from the Developmental Studies Hybridoma Bank, created by the NICHD of the NIH and maintained at the University of Iowa, Department of Biology, 52242. Secondary antibodies Alexa Fluor 488 anti-rabbit (cat.no. 711-545-152, RRID: AB_2313584) or anti-mouse (cat.no. 715-545-151, RRID: AB_2341099) and Cy3 anti-rabbit (cat.no. 111-165-003, RRID: AB_2338000) or anti-mouse (cat.no. 115-165-003, RRID: AB_2338680) were from Jackson ImmunoResearch Laboratories Inc. antibodies.

2.3 | Hippocampal, cortical, and spinal cord acute slices

Acute brain slices (300 μm thick) were prepared from C57BL/6 mice and *SD* rats; acute spinal slices (350 μm thick) were prepared from *SD* rats. Animals were decapitated under inhalation anesthesia with isoflurane (4%–5%). Dissected hippocampi, brain hemispheres, and spinal cords were glued to the platform of a vibroslicer chamber containing ice-cold artificial cerebrospinal fluid (ACSF) whose composition was (in mM): NaCl 134; KCl 2.8; $NaHCO_3$ 29; NaH_2PO_4 1.1; glucose 12; $MgSO_4$ 1.5; $CaCl_2$ 2.5. Transverse hippocampal slices, coronal brain slices comprising the somatosensory cortex, and spinal cord slices from the lumbar area were transferred to a storage chamber where they rested on a nylon mesh, submerged in ACSF at room temperature (RT) for a stabilization period of 45 min before use. The ACSF solution was equilibrated with 95% O_2 and 5% CO_2 (pH 7.4).

2.4 | Whole-mount retinas

Whole-mount retinas were prepared from C57BL/6 mice as reported (Ivanova et al., 2013). To perform retina dissection, enucleated eyes were immersed in physiological saline solution (N-HEPES) containing (in mM): NaCl 135.5; KCl 5.9; $MgCl_2$ 1.2; Hepes 11.6; Glucose 11.5; $CaCl_2$ 1.8 (pH 7.4). Eyes were held by the optic nerve while cutting and removing the cornea and sclera; the iris, lens, and vitreous were pulled out with forceps. The retina was detached from the eyecup and the optic nerve cut. The entire retina was flattened by making 3–6 small incisions in its periphery. After, the whole retina was mounted onto the membrane filter (MF-Millipore™, 0.45 μm pore size, gridded) and incubated in N-HEPES for a stabilization period of 20 min before incubating in TO-PRO-3.

2.5 | Loading spinal and cerebral slices and retinas with TO-PRO-3

Pericytes from acute slices and isolated retinas were labeled with the fluorescent tracer TO-PRO-3 following a previously reported technique with some modifications (Lacar et al., 2012). The general procedure is depicted in Figure 1(a). Unless specified, the dye was added into the ACSF or N-HEPES physiological solutions at 1 μM final concentration from a 1-mM stock solution dissolved in DMSO. Acute slices and whole-mount retinas were incubated at RT in TO-PRO-3-containing ASCF or N-HEPES respectively for 20 min. Then preparations were rinsed for 15 min with physiological solutions to stop dye uptake and reduce background labeling. Afterward, sections were either submerged in fixing solution (4% paraformaldehyde-PFA in PBS; 40 min) or used in living experiments. Fixed slices and retinas were rinsed twice in PBS for 15 min under shaking, labeled with DAPI (1 μM; 10 min), rinsed once again in PBS, and mounted in mounting medium. In few experiments, the dye TO-PRO-3 was applied either by retro-orbital injection of the venous sinus in the eye retro-bulbar space (Yardeni et al., 2011) under inhalation anesthesia (isoflurane 4%–5%) or by intraperitoneal injection; slices were obtained shortly after (30 min–1 hr). In both cases, we found no labeling of TO-PRO-3 in slices. Our study was not pre-registered.

2.6 | Blocking TO-PRO-3 uptake in acute hippocampal slices

In blocking experiments, acute slices were treated with the general Cx/Panx1 inhibitor carbenoxolone (CBX) or the blocking mimetic peptide against pannexin1 (^{10}Panx1) during the last 20 min of uptake recording (Figure 8(a)). The CBX solution was prepared from a 10-mM stock solution dissolved in physiological saline, then applied to slices at 100 μM, whereas ^{10}Panx1 was directly dissolved in ACSF, and administered at 150 μM final concentration.

2.7 | Labeling TO-PRO-3-pre-loaded pericytes with Neurotrace 500/525 in acute brain slices

To evidence colocalization between TO-PRO-3 and NeuroTrace 500/525 labeling, acute hippocampal slices previously loaded

with TO-PRO-3 were incubated at RT for 20 min in ACSF containing the dye NeuroTrace 500/525 (1:25 and 1:500 dilutions). Then slices were washed in ACSF for 15 min and either fixed in fixing solution (PFA, 4%; 40 min) or employed in living experiments (Figure 5, (a) and (c)).

2.8 | Vessel staining

Mice were placed in the chamber of an inhalation anesthesia equipment (VETEQUIP impac 6) and rapidly anesthetized with isoflurane (4%–5%) which presents ample potency and a protective effect in vital tissues (Eger, 2004). The membrane-impermeable dye FITC-dextran (FITC-Dextran-70S; 2–4 mg dissolved in 100 μL of physiological solution) was administered by retro-orbital injection of the venous sinus in the eye retro-bulbar space (Yardeni et al., 2011) by using an insulin needle and syringe. After recovery, the mouse brain was removed to obtain acute hippocampal slices as described above. In another set of experiments, TO-PRO-3 pre-loaded slices were incubated at 37°C with Isolectin B4 (FITC-ISOB4; 5 μg/ml) for 1 hr and then rinsed in ACSF for 15 min. Next, the living slices were fixed in a fixing solution (4% paraformaldehyde in PBS; 40 min) and then rinsed twice for 15 min in PBS. Following washes, slices were exposed for 10 min to 2-[4-(Aminoiminomethyl) phenyl]-1*H*-Indole-6-carboximidamide hydrochloride (DAPI; 1–5 μM diluted in PBST) and rinsed again.

2.9 | Imaging and quantification of TO-PRO-3 uptake

Sections were mounted onto the stage of a confocal microscope (Leica SP5 TANDEM SCANNER) and labeled cells were visualized with a 40x oil immersion objective Leica N.A 1,3 with UV correction. Image stacks were captured with the LAS AF Lite Software in data mode xyz and acquired with appropriate filters for DAPI (excitation/emission 358/461 nm), NeuroTrace (excitation/emission 500/525 nm) or fluorescein (excitation/emission 488/515 nm) and TO-PRO-3 (excitation/emission 642/661 nm). Within the range of fluorescence gain used, we did not appreciate bleeding of TO-PRO-3 emission through other channels. Microscope and camera settings were set to allow measurements within the dynamic range of the fluorescence intensities and remained the same in experiments in which comparisons were made. During living experiments, acute loaded slices were held on the bottom of a homemade flow-through chamber and perfused with ACSF (1 ml/min) equilibrated with a mixture of 95% O_2 and 5% CO_2. To evaluate the impact of different doses of TO-PRO-3 and variations of the temperature on dye uptake, the TO-PRO-3 fluorescence was quantified in arbitrary units (AU) with image processing software Image J (NIH, Bethesda, MD, USA). TO-PRO-3 intensities were evaluated as the difference ($F\text{-}F_0$) between the fluorescence (F) from pericytes and the background fluorescence (F_0) measured in the same field where no labeled cells were detected. At least three fields were selected in every slice.

2.10 | Pericyte morphometry and density

To determine the length and number of longitudinal processes derived from TO-PRO-3-somas, consecutive confocal images of brain adjacent fields were superimposed to allow the reconstruction of pericyte processes. We measured the length of each prolongation from its emergence at the pericyte body until its division into primary branches using the Image J software (NIH, Bethesda, MD, USA). Image stacks of the Stratum Radiatum from hippocampal slices were imported to a software (Adobe Photoshop CS6 13.0 × 64) and z stacks reconstructed and converted to a grayscale mode. Pericyte somas were counted in fields from z stacks reconstructed images; pericyte density was referred to the number of pericytes each mm^3 of brain volume analyzed.

2.11 | Immunofluorescence

To block unspecific sites and permeabilize membranes, fixed preparations pre-loaded with TO-PRO-3 were placed in a multiwell dish and immersed for 2 hr in agitation in a blocking solution containing 2% bovine serum albumin (BSA) and 0.2 M glycine diluted in PBS with 0.5% Triton X-100 (PBST). For α-SMA labeling, before fixing, some slices were incubated for 40 min in Jasplakinoide (20 μM), an F-actin stabilizing reagent that promotes actin filament polymerizing (Alarcón-Martínez et al., 2018; Holzinger, 2009), then rinsed with PBS and fixed either in PFA or in a mixture of 95% methanol and 5% acetic acid (Alarcón-Martínez et al., 2018). After three washes in PBST, fixed slices were incubated at 4°C for at least 24 hr in PBST containing 2% BSA (PBST-BSA) with primary antibodies anti-NG2 (1:250), anti-PDGFrβ (1:150), anti-GFAP (1:400), anti-NeuN (1:200), anti-α-SMA (1:300), and anti-PECAM-1 (1:10). Subsequently, slices were rinsed two times in PBST and incubated in dark for 2 hr in a secondary antibody diluted in the same medium (1:1,000). Following three washes with PBST, slices were treated for 10 min with DAPI (1–5 μM diluted in PBST) and rinsed again. Finally, slices were mounted in glycerol and examined with a confocal laser-scanning microscope (Leica TBCS SP2). Confocal images were acquired with appropriate lasers and using the LAS AF Software in data mode xyz. As a negative control, we omitted primary antibodies. In some trials, to unveil eventually masked antigen epitopes, we performed antigen retrieval for α-SMA labeling by incubating fixed slices at 80°C for 30 min in 10 mM sodium citrate buffer, pH 6.0, before the immunocytochemistry procedure.

2.12 | Cell membrane integrity experiments

To assess the membrane integrity of TO-PRO-3 labeled pericytes, slices were incubated for 20 min in ACSF (95% O_2, 5%

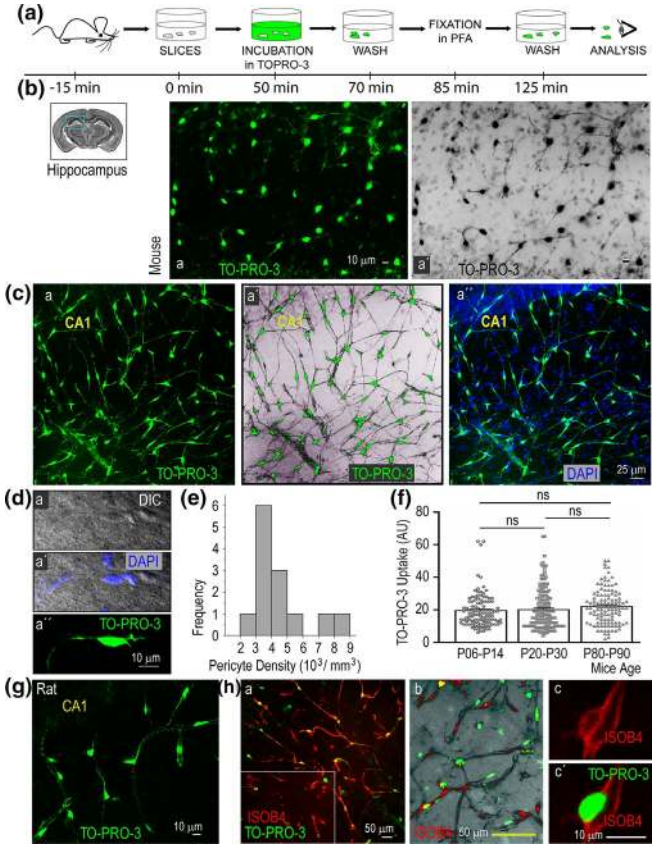

FIGURE 1 TO-PRO-3 labels hippocampal pericyte-like cells in slices of murine. (a) The scheme depicts the temporal course of the experimental procedure designed to label pericytes with TO-PRO-3 in acute brain slices. (b) Left: scheme of a coronal brain slice including the hippocampus (sky blue box). Right: Fluorescent microphotographs of mice hippocampus (z stacks reconstructed images from the Stratum Radiatum; the fluorescent field (picture a) and its inverted fluorescence image (picture a´) illustrate TO-PRO-3$^+$ pericyte-like somas in bright green and black (pictures a and a´ respectively) where cellular morphology and prolongations are evident. (c) Fluorescent microphotographs of mice hippocampus (Stratum Radiatum; same field in pictures a–a´´) show bright TO-PRO-3$^+$ pericyte-like somas (green) giving rise to prolongations that intermix (black in the inverted fluorescent image a´). Cellular nucleus stained with DAPI was merged to (picture a) in (picture a´´). Each image is representative of hippocampi from nine mice. (d) A typical pericyte is depicted by using DIC (Differential interference contrast) microscopy (see a); the DIC image (picture a) was merged to fluorescent images to display the pericyte nucleus marked with DAPI (picture a´) and the soma stained with TO-PRO-3 (picture a´´). Image is representative of hippocampi of three mice. (e) Frequency distribution of the TO-PRO-3$^+$ pericyte-like cells density in mice hippocampus (bin 1000, $n = 13$ hippocampi from 3 mice). (f) TO-PRO-3 uptake by pericyte-like cells of the mouse at different ages. The graph illustrates the TO-PRO-3 uptake (mean ± SEM) in arbitrary units (AU) for pericytes of hippocampal slices derived from mice from three different age ranges; (P06-P14, $n = 112$ pericytes from 3 mice; P20-P30, $n = 174$ pericytes from 3 mice; P80-P90, $n = 117$ pericytes from 3 mice). ns, non-significant, comparison between 2 values indicated by horizontal bars, Kruskal–Wallis-test followed by Dunn post-test. Each dot represents the uptake value for a single cell. (g) TO-PRO-3 labels pericyte-like cells in rat hippocampus (Stratum Radiatum). The fluorescent image is representative of the hippocampi of six rats. (h) TO-PRO-3-labeled cells line up to the brain vasculature. Two different hippocampal areas displayed in fluorescent (picture a) and inverted fluorescent (picture b) images illustrate TO-PRO-3 stained pericyte-like cells in close association with vessels marked by Isolectin B_4 conjugated to fluorescein (FITC-ISOB4). Basement membranes of endothelium and pericytes marked by FITC-ISOB4 outline TO-PRO-3-labeled somas (same field in pictures c–c´). Images are representative of three mice. In all these examples, fixed slices are shown

CO_2; pH 7.4) containing the membrane non-permeant FITC-dextran (FITC-Dextran-70000 kDa; 5 mg/ml). Subsequently, slices exposed to FITC-dextran were fixed (4% paraformaldehyde in PBS; 40 min), rinsed in PBS, and mounted in mounting medium until photomicrographs were taken. Labeled pericytes were visualized with a confocal laser-scanning microscope (Leica TBCS SP2) with filters appropriate for FITC (excitation/emission maxima 489/515 nm).

2.13 | Statistics

Values are presented as mean ± *SEM*. Analysis of distribution was done before a statistical test, using GraphPad InStat 3.06 (California Corporation). In cases where sample distribution did not pass the normality test (KS), non-parametric data were analyzed using two-tailed Mann–Whitney test and Kruskal–Wallis test followed by Dunn post-test. In all experiments, the level of significance was set at $p < .05$. Sample sizes were estimated based on reports assessing dye uptake; these require 3–4 slices per condition per animal and a minimum of three mice per condition (Abudara et al., 2015; Garré et al., 2010); no sample calculations were done. Statistical analysis/graphics were performed with the GraphPad InStat 3.06 (California Corporation) software; figures were prepared with Adobe Photoshop CS6 13.0 × 64 and Adobe Illustrator CS6 16.0.0. We conducted no test for outliers.

3 | RESULTS

3.1 | TO-PRO-3 strongly labels pericyte-like cells in the murine neurovascular unit

Incubation of acute hippocampal slices in TO-PRO-3-containing ACSF (Figure 1(a)) resulted in robust labeling of a subset of pericyte-like cells that strongly incorporated the fluorophore (TO-PRO-3$^+$ cells). The dye concentrated at spindle-shaped cellular bodies but also traced cellular processes (Figure 1, (b)–(d)) that intermixed in an extensive meshed network (Figure 1(c)a´). The bright staining displayed by TO-PRO-3$^+$ cells was remarkably higher than the background, defined as the area devoid of marked cells, which gave a significant signal-to-noise ratio. The fluorescence intensity (mean ± *SEM*) measured at the soma (F) was 41.93 ± 1.96 (Arbitrary Units or AU), whereas the background fluorescence (F_0) was 1.96 ± 0.09 AU ($p < .0001$,

Wilcoxon matched paired test; $n = 123$ TO-PRO-3$^+$ cells from 4 mice); the mean signal-to-background ratio F/F_0 was 50.3 times. Usually, healthy slices showed high F/F_0 ratios. Fixed sections stored at 4°C, preserved the bright stain for at least 1–1.5 months. Increasing the fluorescence intensity gain revealed TO-PRO-3$^+$-nucleoli in pyramidal neurons but solely pericyte-like cells displayed bright and extensive labeling. In mouse hippocampi, the mean density of TO-PRO-3$^+$ pericyte-like cells was 4,454 ± 451 cells/mm^3, most density values ranged between 3x10^3 and 5x10^3 TO-PRO-3$^+$ cells/mm^3 ($n = 13$ hippocampi from 9 mice) (Figure 1(e)). These values were consistent with the densities of pericytes previously identified with NeuroTrace 500/525 (Damisah et al., 2017). Although we typically used P20-P30 mice, TO-PRO-3 also labeled pericyte-like cells at earlier stages of development (P06-P14 mice) and during adulthood (P80-90 mice) (Figure 1(f) and S1). Quantification of TO-PRO-3 uptake by TO-PRO-3$^+$ pericyte-like cells yielded (mean ± *SEM*) 19.5 ± 0.97 AU for P06-P14 mice ($n = 112$ cells from 3 mice), 20.1 ± 0.92 AU for P20-P30 mice ($n = 174$ cells from 3 mice), and 21.96 ± 0.99 AU for P80-P90 mice ($n = 117$ cells from 3 mice). We found no differences between these groups (ns: non-significant, Kruskal–Wallis-test followed by Dunn post-test) (Figure 1(f)). In addition to mouse areas, TO-PRO-3 also stained pericyte-like cells in the hippocampus and spinal cord of rats (Figure 1(g); Figure S2).

The TO-PRO-3$^+$ pericyte-like cells typically aligned to the cerebrovasculature, specifically to the smallest caliber vessels, presumably capillaries (Figures 1(h) and 2). Figure 1(h) displays the close association between labeled cells and vessel walls identified by FITC-ISOB4 which specifically binds to α-D-galactose residues in basement membranes of endothelium and pericytes (Laitinen, 1987; Peters & Goldstein, 1979; Mishra et al., 2014). As expected, FITC-ISOB4 staining outlined the somas of TO-PRO-3$^+$ pericyte-like cells (Figure 1(h), c-c´). Figure 2, (a)–(c´) depicts the general arrangement of TO-PRO-3$^+$ cells in adjacency to thin hippocampal vessels. Figure 2(d)c illustrates a representative labeled soma juxtaposed to the abluminal wall of a capillary presenting a diameter less than 10 μm and devoid of a continuous layer of αSMA; conversely, TO-PRO-3$^+$ cells did not show intimate association to arterioles (see picture (d)b).

Cells labeled by TO-PRO-3 exhibited the distinctive morphological features of pericytes; somas were fusiform while giving rise to slim prolongations that extended several micrometers away as it is characteristic of pericytes (Figure 3). The TO-PRO-3$^+$ prolongations originated from somas projected longitudinally along vessels (Figure 3, (a) and (b), arrowheads) while branching out to new processes (Figure 3, (a) and (b), arrows). The length of the longitudinal TO-PRO-3$^+$ processes derived from somas ranged between 2 and 110 μm and the majority (63%) measured between 12 and 42 μm ($n = 142$ processes from 7 mice) (Figure 3(c)). The characteristic fusiform cell bodies of TO-PRO-3$^+$ cells were also found in other areas of the nervous system including the somatosensory cortex (Figure S1), the spinal cord (Figure S2), and the retina (Figure S3). In the mouse retina, however, labeling seemed to span other cell types, mostly at the emergence of the optic nerve (not shown).

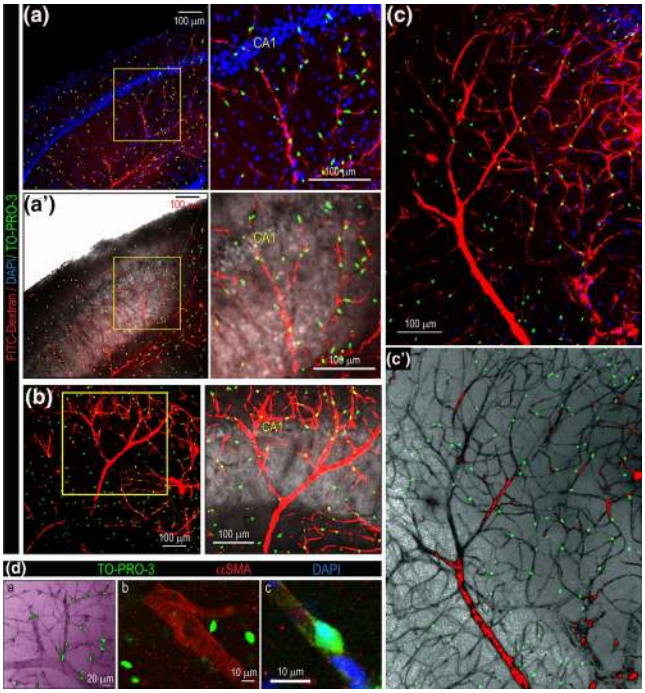

FIGURE 2 TO-PRO-3-labeled cells align with blood microvessels. (a) and (b) Left panels represent panoramic views of mice hippocampus with TO-PRO-3-labeled pericyte-like cells associated with the brain vasculature. Right panels depict zoomed areas framed by yellow boxes in left pictures. Fluorescent images showing TO-PRO-3-stained pericytes and FITC-Dextran-marked vessels in (a) and (b) were merged to their respective DIC versions in (a´) and the zoomed view of the selected area in (b); note the scarcity of pericytes adjacent to large vessels. (c) and (c´) TO-PRO-3$^+$ cells associate with thin vessels. A general view of a hippocampal area illustrates TO-PRO-3-labeled cells resting on thin FITC-Dextran-marked vessels; the inverted fluorescent version (c´) of the fluorescent field (c) allows visualization of small vessels. (d) TO-PRO-3$^+$ cells rest on capillaries but not on arterioles. The inverted fluorescent picture (picture a) aims to show pericyte somas (green) associated with small diameter vessels (contours of vessels in dark violet). Fluorescent photographs of mice hippocampus display brightly TO-PRO-3$^+$ cells unrelated to α–SMA$^+$ arterioles (picture b) and a TO-PRO-3-labeled pericyte soma adjacent to a microvessel (picture c). Each image is representative of five mice

In summary, based on their morphology, perivascular location, and abundance, the TO-PRO-3$^+$ cells from the murine nervous system, looked like pericytes.

To confirm the identity of TO-PRO-3$^+$ cells, we first addressed the specificity of TO-PRO-3 labeling by immunofluorescence. To do so, mice hippocampal slices previously loaded with TO-PRO-3 were counter-immunostained with antibodies against the classical pericyte markers transmembranous chondroitin sulfate proteoglycan neuron-glial antigen 2 and the platelet-derived growth factor receptor beta antigen (Figure 4(a)) (Hartmann, et al., 2015a,b; Lindahl et al., 1997; Ozerdem et al., 2001; Smyth et al., 2018). In the hippocampus, the majority of TO-PRO-3$^+$ cells showed co-labeling with PDGFrβ or NG2; the immunostaining pattern for both markers displayed a preferential distribution at the cell membrane unlike

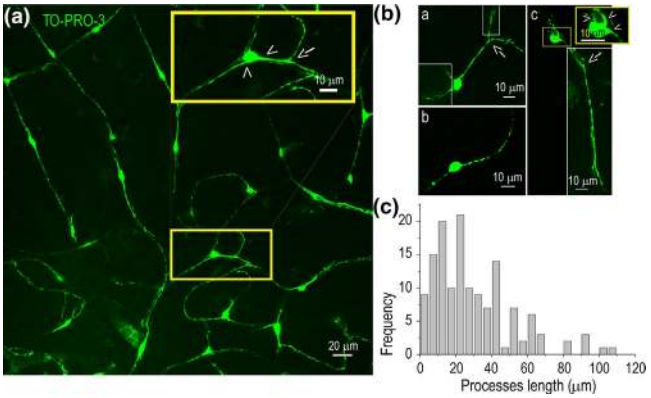

FIGURE 3 TO-PRO-3 images cellular prolongations of pericyte-like cells in mouse hippocampus. (a) The fluorescent photograph displays a representative field of Stratum Radiatum with TO-PRO-3 brightly labeled pericyte-like somas that originate primary longitudinal prolongations (arrowheads in zoomed yellow box) giving rise to secondary processes (arrow in zoomed yellow box). (b) Fluorescent views depict hippocampal pericyte somas giving rise to TO-PRO-3$^+$ processes (pictures a–c); to aid visualization of prolongations, the level of fluorescence was increased within white boxes. Arrowheads indicate the emergence of primary processes from pericytes somas in the zoomed area (yellow box in picture c); arrows point out the sites of bifurcations (pictures a and c). (c) Frequency distribution for primary processes length (in μm) of TO-PRO-3$^+$ pericytes (bin 5, n = 142 pericytes from 7 mice)

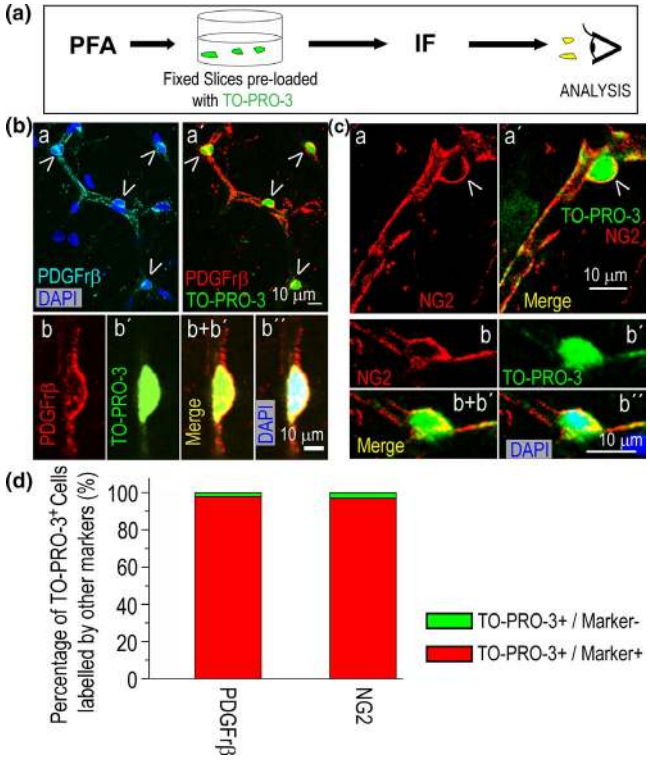

FIGURE 4 Pericyte markers stain TO-PRO-3$^+$ cells in mouse hippocampus. (a) The diagram illustrates the procedure employed to stain pericytes with TO-PRO-3 and immunomarkers. (b) and (c) Fluorescent images display TO-PRO-3$^+$ cells co-stained with (b) PDGFrβ (same fields in pictures a-a´ and b-b´´) and (c) NG2 (same fields in pictures a-a´ and b-b´´). Arrowheads (in pictures a-a´) point out pericytes contiguous to cerebral vessels that protrude reminding the typical "bump-on-a-log" placement of pericytes. Each image is representative of four mice. (d) The graph represents the percentage of hippocampal TO-PRO-3$^+$ cells co-labeled with the markers PDGFrβ (n = 222 TO-PRO-3$^+$ cells of 49 fields from 5 mice) and NG2 (n = 90 TO-PRO-3$^+$ cells of 22 fields from 3 mice)

TO-PRO-3, which labeled the whole cell body (Figure 4, (b) and (c)). The TO-PRO-3$^+$ cells protruded from the outer wall of blood vessels reminding the typical "bump-on-a-log" placement of pericytes (Rouget, 1873) (arrowheads in Figure 4, (b) and (c)). In tissue sections, we found that 98% of TO-PRO-3$^+$ cells were co-labeled with PDGFrβ (n = 222 TO-PRO-3$^+$ cells of 49 fields from 5 mice) while 97% of TO-PRO-3$^+$ cells were co-labeled with NG2 (n = 90 TO-PRO-3$^+$ cells of 22 fields from 3 mice) (Figure 4(d)). Importantly, most cells identified as pericytes captured TO-PRO-3. Accordingly, 91% of PDGFrβ$^+$ cells adjacent to capillaries incorporated TO-PRO-3 (n = 244 PDGFrβ$^+$ cells of 39 fields from 3 mice), 84% of NG2$^+$ cells associated to vessels took up TO-PRO-3 (n = 110 NG2$^+$ cells of 18 fields from 3 mice), whereas 99% of double-labeled PDGFrβ$^+$/NG2$^+$ cells were TO-PRO-3$^+$ (n = 88 PDGFrβ$^+$/NG2$^+$ cells of 30 fields from 3 mice).

A previous report has recently shown that the Green Fluorescent Nissl dye NeuroTrace 500/525 which usually stains neurons in fixed brain sections, identifies pericytes in vivo as distinct vascular mural cells, different from VSMCs (Damisah et al., 2017). We took advantage of this in vivo approach to label pericytes and adapted it to acute brain slices that we used in living or fixed experiments (procedures in Figure 5, (a) and (c)). In slices, the NeuroTrace 500/525 staining concentrated at the soma and primary processes similarly as TO-PRO-3 (Figure 5, (b), (d) and (e)). About 95% of TO-PRO-3$^+$ cells in hippocampus took up NeuroTrace 500/525 (n = 442 TO-PRO-3$^+$ cells of 55 fields from 4 mice) (Figure 5(f)). Double-labeled TO-PRO-3$^+$/NeuroTrace500/525$^+$ cells were associated with blood vessels whose walls were occasionally delineated by prolongations (Figure 5(e)b´´´). During living experiments (up to 6 hr duration), TO-PRO-3$^+$ cells showed no signs of toxicity (cellular disintegration, swelling or shrinkage) and morphological features remained stable. In time-lapse experiments, NeuroTrace 500/525 displayed a greater photostability than TO-PRO-3 labeling.

In summary, our findings demonstrated that hippocampal TO-PRO-3$^+$ cells expressed the classical pericyte immunomarkers NG2 and PDGFrβ and captured the pericyte dye NeuroTrace 500/525 providing evidence that they represented cerebral pericytes.

3.2 | The contractile protein α-SMA is detected in TO-PRO-3$^+$ cells

Consistent with the idea that capillary pericytes play a regulatory role in microcirculation, these cells are expected to express the contractile protein α-SMA. Herein, we employed different strategies to identify α-SMA in hippocampal TO-PRO-3$^+$ pericytes. Results were exemplified and summarized in Figure 6. Classical immunocytochemistry applied to hippocampal slices pre-loaded with

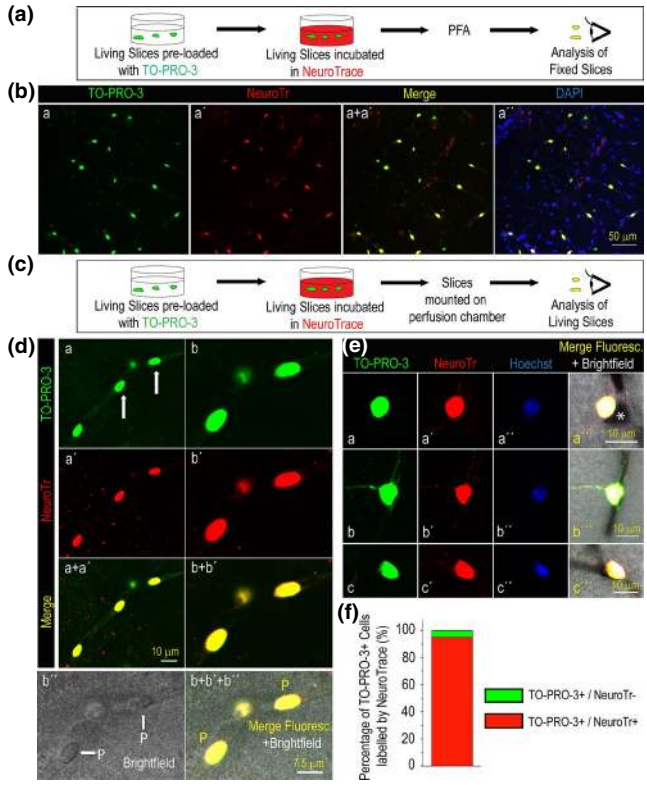

FIGURE 5 The pericyte marker NeuroTrace 500/525 stains TO-PRO-3-labeled cells in mouse hippocampus. Co-localization between NeuroTrace 500/525 and TO-PRO-3 is visualized in both fixed and living slices. (a) The diagram illustrates the experimental process employed to label pericytes with TO-PRO-3 and NeuroTrace 500/525 in hippocampal slices. Note that incorporation of both dyes into pericytes should be achieved in living tissue; slices were then fixed and analyzed. (b) Fluorescent pictures depict fixed slices with pericytes stained with TO-PRO-3 (picture a) and NeuroTrace 500/525 (picture a´) in mice hippocampus (same field in a-a´´; co-labeling in a+a´ and a´´ where the DAPI image was merged). (c) The diagram illustrates the experimental process employed to label hippocampal pericytes with TO-PRO-3 and NeuroTrace 500/525 in acute sections; living slices were then imaged and analyzed through confocal microscopy. (d) Representative fluorescent and brightfield pictures of mice hippocampal living slices display pericytes stained with TO-PRO-3 (green) and NeuroTrace 500/525 (red); co-labeling is shown in yellow. Same field in pictures (a-a+a´). Two pericytes indicated by arrows (picture a) were zoomed (b–b+b´+b´´; same field). P: pericyte (b´´; b+b´+b´´). (e) Fluorescent pictures depict three different living pericapillar pericytes stained with TO-PRO-3 (green) and NeuroTrace 500/525 (red) in mouse hippocampus. Images in each file represent the same field. Note pericytes adjacent to vessels in brightfield views (a´´´, b´´´ and c´´´); the asterisk indicates blood accumulation in a vessel bifurcation (a´´´). Each image is representative of four mice. (f) The graph represents the percentage of TO-PRO-3+ cells co-labeled with NeuroTrace 500/525 (n = 442 TO-PRO-3+ cells of 55 fields from 4 mice)

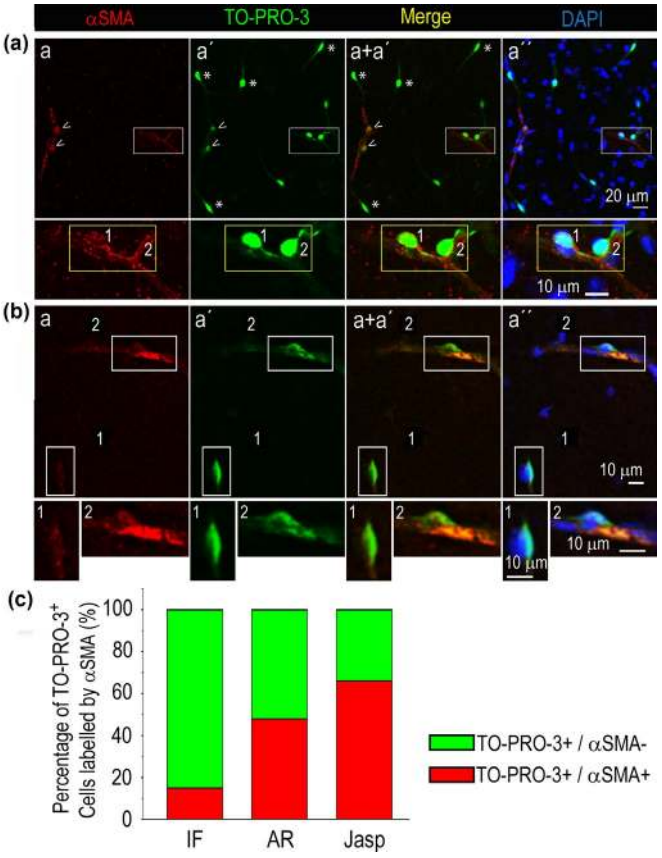

FIGURE 6 TO-PRO-3 pericyte-like cells express α-SMA. (a) Fluorescent pictures (a-a´´, same field) of pericyte-like cells identified with TO-PRO-3 show the expression of α-SMA detected through conventional immunofluorescence. Note that pericytes resting on α-SMA-expressing vessels (arrowheads in a-a+a´) exhibit larger levels of α-SMA stain than pericytes adjacent to non-expressing α-SMA structures (asterisks in pictures a´-a+a´). The field within the white rectangle (pictures a-a´´) was zoomed and is shown below. In zoomed views, the level of fluorescence was increased within the yellow boxes to visualize an α-SMA-expressing TO-PRO-3$^+$ cell (α-SMA$^+$; cell 1) next to a non-expressing TO-PRO-3$^+$ cell (α-SMA$^-$; cell 2). (b) Fluorescent pictures (a-a´´, same field) show the expression of α-SMA by TO-PRO-3$^+$ pericyte-like cells (1 and 2) detected through the antigen retrieval procedure. Fields within white rectangles (a-a´´) were zoomed and are shown below. Note the strong stain of α-SMA in pericyte 2 adjacent to the α-SMA-expressing vessel as compared to pericyte 1. Note in (a) and (b) that TO-PRO-3$^+$ cells displaying more stain for α-SMA exhibit lower levels of TO-PRO-3 than TO-PRO-3$^+$ cells with low or no labeling for α-SMA. (c) The graph represents the percentage of hippocampal TO-PRO-3$^+$ cells co-labeled with α-SMA. IF: α-SMA detected by conventional immunofluorescence (n = 106 TO-PRO-3$^+$ cells of 12 fields from 3 mice); AR: α–SMA detected by antigen retrieval (n = 105 TO-PRO-3$^+$ cells of 40 fields from 3 mice) and Jasp: α-SMA detected by immunofluorescence in slices pretreated with jasplakinolide (n = 114 TO-PRO-3$^+$ cells of 17 fields from 3 mice)

TO-PRO-3 yielded immunoreactivity against the α-SMA antibody in uniquely the 15% of TO-PRO-3$^+$ cells (n = 106 TO-PRO-3$^+$ cells of 12 fields from 3 mice). Performing antigen retrieval on fixed hippocampal slices before incubation with the anti-α-SMA primary antibody allowed us to detect α-SMA-positive immunoreaction in 48% of TO-PRO-3$^+$ cells (n = 105 TO-PRO-3$^+$ cells of 40 fields from 3 mice). Finally, precluding eventual depolymerization of α-SMA by pre-treating hippocampal slices with jasplakinolide before fixation

(Alarcón-Martínez et al., 2018; Holzinger, 2009), further enhanced the total number of double-labeled α-SMA$^+$/ TO-PRO-3$^+$ cells by 66% (n = 114 TO-PRO-3$^+$ cells of 17 fields from 3 mice).

In summary, we found here that TO-PRO-3$^+$ pericytes from hippocampal slices were able to express α-SMA under specific immunohistochemical conditions.

3.3 | TO-PRO-3$^+$ cells associate to other components of the neurovascular unit

To investigate whether TO-PRO-3$^+$ cells relate to other constituents of the NVU, hippocampal sections were counter-immunostained with specific antibodies against neurons, astrocytes, and endothelium (Figure 7). Figure 7(a) illustrates hippocampal TO-PRO-3$^+$ pericytes neighboring CA1 pyramidal neurons; the neuron-specific nuclear protein NeuN imaged hippocampal CA1 neurons, as expected we observed no matching between NeuN$^+$ and TO-PRO-3$^+$ cell populations (picture c). Likewise, we found non-overlapping labeling patterns between TO-PRO-3 and the glial fibrillary acidic protein (GFAP), a specific marker of astrocytes (Figure 7(b)). At the NVU, pericytes, vessels and astrocytes are intimately related. In line with this, GFAP$^+$ astrocyte processes either enwrapped TO-PRO-3$^+$ cells juxtaposed to the vessel wall or contacted the vessel in the vicinities of pericytes (Figure 7(b)b). As is typical for pericytes, TO-PRO-3$^+$ cells rested on the abluminal wall of vessels as shown in Figure 7(c) where the vascular endothelium was identified with the specific antibody against the platelet endothelial cell adhesion molecule (PECAM-1).

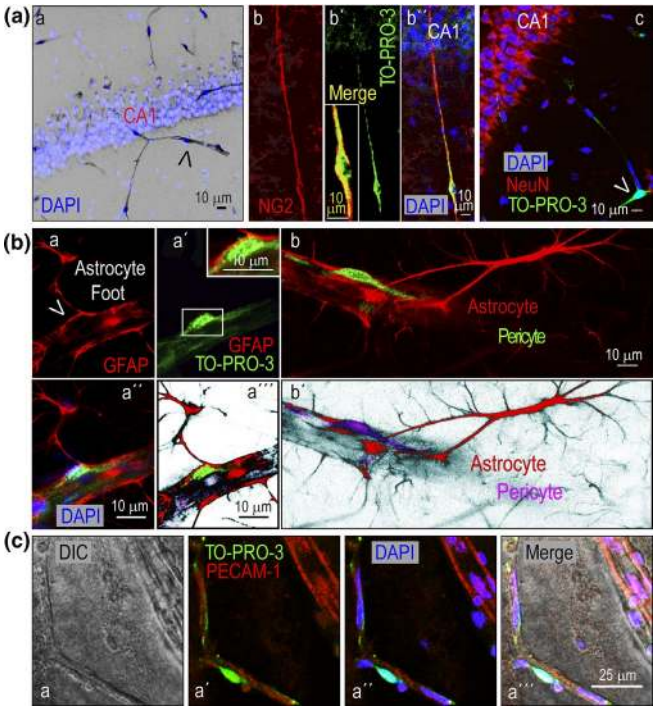

FIGURE 7 TO-PRO-3$^+$ pericyte-like cells are components of the neurovascular unit in mouse hippocampus. (a) Fluorescent images display pericytes stained with DAPI (arrowhead in picture a) and with TO-PRO-3 (b´; arrowhead in c) and NG2 (b-b´´, same field) neighboring CA1 pyramidal neurons. In picture c, neuronal bodies were immunolabeled with the neuronal marker NeuN; the nucleus of CA1 pyramidal neurons stained with DAPI are evident in pictures a, b´´ and c (b) Fluorescent images depict the rapport between TO-PRO-3-labeled pericytes and astroglial GFAP-stained prolongations. An astrocyte foot enwraps a pericyte soma, which rests on a blood vessel (a-a´´´, same field), whereas astrocyte feet contact vessel walls neighboring a pericyte lying on the vessel (b-b´, same field). Inverted fluorescent pictures a´´´ and b´ aim to facilitate the visualization of relationships between pericytes, astrocyte feet and vessel walls. (c) Pictures illustrate a TO-PRO-3-labeled pericyte lining up endothelial cells stained with PECAM-1 (a-a´´´, same field). The DIC field (picture a) was merged to the fluorescent image (a´´) in (a´´´). Each image is representative of three mice

3.4 | Which mechanisms underlie the passage of TO-PRO-3 through the pericyte membrane at the NVU?

The fluorophore TO-PRO-3 (MW 671.4 g/mol) is cell impermeant (Suzuki et al., 2007) and therefore requires relatively large pores to diffuse through the membrane or else a transport mechanism to enter into cells when applied extracellularly. Neither the injection of TO-PRO-3 in the retro-orbital venous sinus nor the intraperitoneal injection of TO-PRO-3 yielded labeled cells.

We first ruled out the possibility that the membrane integrity of TO-PRO-3$^+$ cells has been impaired allowing the passage of relatively large molecules through an altered lipid bilayer. For this, we incubated slices in ACSF solution containing the membrane non-permeant FITC-dextran (70 000 kDa). The FITC-dextran disposed outside pericytes and delineated the silhouette of the TO-PRO-3$^+$ cell somas suggesting that an intact membrane impeded the entry of the dye into pericytes (Figure S4).

We then assessed the possible contribution of large pore membrane channels formed by pannexin1 (Panx1-pannexons) or connexin43 (Cx43 hemichannels or connexons); in other systems, pannexons act as pathways for TO-PRO-3 influx (Chekeni et al., 2010; Chiu et al., 2017; Good et al., 2018; Poon et al., 2014). To do so, in acute hippocampal slices, we evaluated the effects of the general Cx/Panx1 inhibitor, carbenoxolone (CBX; 100 μM) (Ma et al., 2009) and the Panx1 blocker, the mimetic peptide ^{10}Panx1 (150 μM) (Pelegrin & Surprenant, 2006) on TO-PRO-3 uptake (Figure 8(a)a). None of these blockers, CBX or ^{10}Panx1 prevented the capture of TO-PRO-3. The TO-PRO-3 uptake ratios for CBX and ^{10}Panx1 treatments, respectively, 1.02 ± 0.03 (n = 302 pericytes from 4 mice) and 0.99 ± 0.03 (n = 291 pericytes from 4 mice) were not different from control, 1.00 ± 0.03 (n = 424 pericytes from 4 mice) (non-significant as compared to control, Kruskal–Wallis-test followed by Dunn post-test) (Figure 8(a)b). These results indicated that non-opposed Cx43 hemichannels and Panx1 channels were

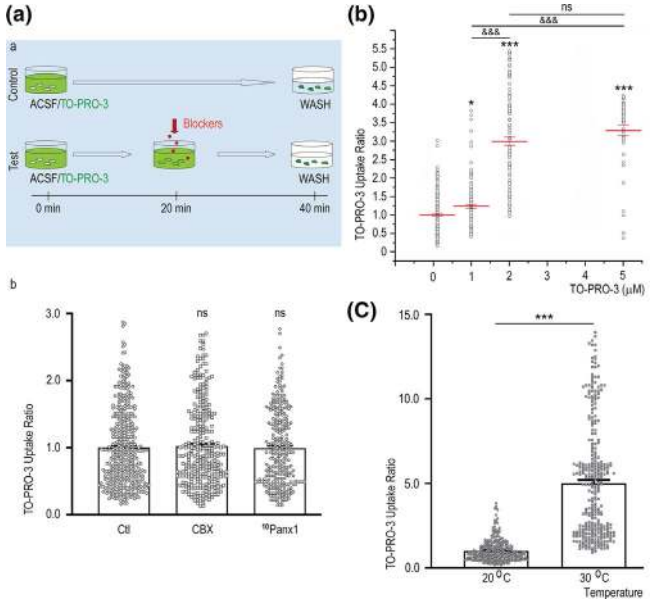

FIGURE 8 Mechanisms underlying TO-PRO-3 uptake by pericytes from mouse hippocampus. (a) Connexin hemichannels and pannexin channels are not the main pathways for TO-PRO-3 influx into mouse cerebral pericytes. a, Diagrams represent the experimental procedure employed to evaluate whether TO-PRO-3 uptake by hippocampal pericytes is mediated via Cx-hemichannels/pannexons. b, The graph illustrates TO-PRO-3 uptake ratios (mean ± SEM) for control (n = 424 pericytes from 4 mice), CBX-treated (n = 302 pericytes from 4 mice), and ^{10}Panx1-treated (n = 291 pericytes from 4 mice) pericytes. Uptake values were normalized to the control mean. Each dot represents the value of an individual TO-PRO-3$^+$ pericyte. ns; non-significant as compared to control, Kruskal–Wallis-test followed by Dunn post-test. (b) TO-PRO-3 uptake by mouse hippocampal pericytes shows saturation. The graph illustrates the TO-PRO-3 uptake ratios (mean ± SEM) for pericytes exposed for 20 min to different doses (0.1–5 μM) of TO-PRO-3 (0.1 μM, n = 218 pericytes from 6 mice; 1 μM, n = 132 pericytes from 3 mice; 2 μM, n = 130 pericytes from 6 mice; 5 μM, n = 49 pericytes from 3 mice). Each dot represents the ratio for a single pericyte. Uptake values were normalized to the mean obtained at the lower dose (0.1 μM). *p < .05; ***p < .001; as compared to 0.1 μM; ns, non-significant; &&& p < .001, comparison between 2 values indicated by horizontal bars, Kruskal–Wallis-test followed by Dunn post-test. (c) Uptake of TO-PRO-3 by hippocampal pericytes is temperature dependent. The graph illustrates TO-PRO-3 uptake ratios (mean ± SEM) for pericytes obtained during incubation of slices in TO-PRO-3-containing ACSF at 20°C (n = 314 pericytes from 6 mice) and 30°C (n = 324 pericytes from 6 mice). Each dot represents the ratio for a single pericyte. Uptake values were normalized to the mean obtained at 20°C. ***p < .001, Mann–Whitney test (two-tail)

not the main routes for dye incorporation suggesting that an additional mechanism might account for TO-PRO-3 entry into brain pericytes.

As an approach to characterize the transport of TO-PRO-3 into pericytes, we evaluated the dye uptake kinetics, by determining the effects of different concentrations of TO-PRO-3 on uptake after 20 min of exposure. Increasing TO-PRO-3 concentrations (0.1, 1, 2, and 5 μM) yielded increasing levels of the uptake ratio until a maximum rate of transport was achieved between 2 and 5 μM, respectively, 2.99 ± 0.11 (n = 130 pericytes from 6 mice) and 3.29 ± 0.14 (n = 49 pericytes from 3 mice) (ns, non-statistically different, Kruskal–Wallis test followed by Dunn post-test) (Figure 8(b)). The maximal capacity to uptake TO-PRO-3, which reflected a saturation of the transport mechanism, suggested that an integral membrane protein (channel or carrier) contributed to transfer the dye into pericytes; this could have happened through either a facilitated diffusion or an active transport (Berne and Levy, 2008; Albert et al., 2002). To discriminate between both mechanisms, we assessed the effect of the temperature on TO-PRO-3 uptake. The mean uptake ratio at 30°C, 5.02 ± 0.18 (n = 324 pericytes from 6 mice) was significantly higher than the one at 20°C, 1.00 ± 0.04 (n = 314 pericytes from 6 mice) (p < .001, two tail Mann–Whitney test) (Figure 8(c)). Consequently, the calculated temperature coefficient or Q10, that is, the factor by which the mean uptake changed upon a 10°C increase in temperature (from 20°C to 30°C), was 5.02. This magnitude of QI0 indicated that TO-PRO-3 uptake was highly sensitive to temperature and suggested that the transport mechanism could have involved protein conformational changes and energy expenditure.

In summary, based on our findings, we suggest that pericytes selectively captured TO-PRO-3 through an active protein-transport mediated system.

4 | DISCUSSION

In the present study, we demonstrate that the fluorescent nuclear tracer TO-PRO-3 Iodide (642/661) acts as a specific dye to image capillary pericytes at the NVU of murine. After brief exposure, the fluorophore was preferentially incorporated by pericytes in live slices of the cortex, hippocampus, spinal cord, and whole-mount retinas. Selective uptake of TO-PRO-3 by cerebral pericytes has been previously reported in the mice subventricular zone from acute slices where TO-PRO-3-loaded pericytes were used for calcium imaging and immunohistochemistry post-fixation (Lacar et al., 2012). However, to our knowledge, a comprehensive study of TO-PRO-3 imaging of pericytes has not been further described.

Different pieces of evidence here obtained indicate that TO-PRO-3 specifically labels pericytes at the neurovascular interface. First, morphological features, that is, protruding spindle-shaped TO-PRO-3$^+$ somas giving origin to longitudinal processes, were typical of pericytes. In line with this, Isolectin B4 that labels the basement membrane, which encloses pericytes (Mishra et al., 2014), delineated TO-PRO-3$^+$ pericyte-like cells and disclosed their perivascular location. Besides, the length of primary longitudinal processes of TO-PRO-3$^+$ cells agreed with those published for pericytes of cortices from the NG2-tdTomato transgenic mouse Cre line, which is driven by the promoter for the NG2 proteoglycan to target pericytes (Hartmann, et al., 2015a,b; Ozerdem et al., 2001). Second, TO-PRO-3$^+$ cells exhibited the classical intimate apposition to microvasculature and the characteristic anatomical rapports shown by pericytes at the NVU. Accordingly, TO-PRO-3$^+$ cells leaned on the

vasculature in close association to astrocyte feet and vessel endothelium to which they partially enwrapped. Assembly between pericytes, vessels and astrocytes is known to favor the exchange across the blood–brain interface (Mathiisen et al., 2010) that is crucial for BBB functions (Abbott et al., 2010). By using electronic microscopy 3D reconstruction in CA1 rat hippocampus, other authors showed that about one-third of endothelium is covered by pericytes (somas and processes), whereas most of the abluminal surface of pericytes is covered by astrocyte endfeet (Mathiisen et al., 2010). Recent data indicate that the vessel coverage depends on the pericyte morphology and vascular territory being maximum (95%) for ensheathing pericytes at pre-capillary arterioles and minimum (51%) for thin-strand pericytes at small diameter capillaries (Grant et al., 2019). Third, TO-PRO-3$^+$ cells expressed NG2 and PDGFrβ antigens, classical markers of pericytes (Hartmann, et al., 2015a,b; Lindahl et al., 1997; Ozerdem et al., 2001; Smyth et al., 2018) and captured the recently described pericyte dye NeuroTrace 500/525 that is exclusively taken up by in vivo pericytes (Damisah et al., 2017). Fourth, almost all cells identified as pericytes (i.e., double-labeled NG2/PDGFrβ cells associated with vessels), were stained by TO-PRO-3. Finally, the abundance of TO-PRO-3$^+$ cells was in line with the densities of cortical pericytes as determined by NeuroTrace 500/525 labeling (Damisah et al., 2017).

A subset of TO-PRO-3$^+$ pericytes expressed the contractile protein α-SMA. In line with a previous report (Alarcón-Martínez et al., 2018), preventing F-actin depolymerization allowed us to identify a larger percentage of α-SMA-expressing TO-PRO-3$^+$ cells (α-SMA$^+$ pericytes) than antigen retrieval or classical immunofluorescence. Despite this, we could not detect the protein in a pool of TO-PRO-3$^+$ cells (α-SMA$^-$ pericytes). The differential expression of α-SMA exhibited by TO-PRO-3$^+$ cells might reflect the heterogeneity of the pericyte population already described by others. Accordingly, ensheathing pericytes at pre-capillary arterioles and capillary pericytes closer to the arteriole end of capillaries would express more α-SMA than mid-capillary ones (Nehls & Drenckhahn, 1991; Ehler et al., 1995; Bandopadhyay et al., 2001; Attwell et al., 2016; Grant et al., 2019). Although we did not perform additional studies to address the precise location of α-SMA-expressing TO-PRO-3$^+$ cells within the vascular tree, our data suggested that both the capillary pericytes close to arterioles (α-SMA$^+$ pericytes) and those located in the mid-capillary bed (α-SMA$^-$ pericytes) captured TO-PRO-3 (Figure 2; Figure 6). Moreover, pericytes located near the arteriole could exhibit lower levels of TO-PRO-3 uptake than pericytes located in the mid-capillary bed (Figure 6, (a) and (b)). Previous work suggested that NeuroTrace 500/525 and α-SMA labeling are inversely related (Grant et al., 2019).

While some groups successfully detected α-SMA in capillary pericytes through IHC procedures and quantitative immunoblotting (Le Beux and Willemot, 1978; Bandopadhyay et al., 2001; Alarcón-Martínez et al., 2018), others obtained negative results by using antibody staining (Grant et al., 2019) or reporter lines driven by α-SMA promoters (Damisah et al., 2017; Hill et al., 2015). This discrepancy could be because of experimental procedures regarding differences in the sensitivity of the detection methods employed (Alarcón-Martínez et al., 2018) or in definition of pericytes (Attwell et al., 2016; Hill et al., 2015; Grant et al., 2019; Grutzendler and Nedergaard, 2019). Alternatively, it may be because of the differential expression pattern of α-SMA exhibited by some preparations (Ehler et al., 1995; Hill et al., 2015; Smyth et al., 2018; Nortley et al., 2019).

The presence of contractile machinery is consistent with pericyte function to actively modify their tone and modulate the capillary diameter and blood flow (CBF) (Kawamura et al., 2003; Peppiatt et al., 2006; Lacar et al., 2012; Hall et al., 2014; Mishra et al., 2016; Kisler, et al., 2017; Isasi et al., 2019; Nortley et al., 2019; Kisler et al., 2020; Nelson et al., 2020; Hartmann et al., 2020 Preprint; Ivanova et al., 2020 Preprint) although this role has not been established by some studies (Fernández-Klett et al., 2010; Hill et al., 2015; Wei et al., 2016). It is accepted that ensheathing pericytes from pre-capillary arterioles express α-SMA and regulate blood flow (Hill et al., 2015; Hartmann et al., 2020 Preprint) but the mechanisms underlying the contractility of mid-capillary pericytes involved in CBF regulation remain unknown. How to reconcile that mid-capillary pericytes regulate the CBF if they express low or undetectable levels of α-SMA? Interestingly, recent papers have proposed that pericytes may use alternative contractile proteins (Nelson et al., 2020; Hartmann et al., 2020 Preprint) expressed by them as determined by transcriptomic studies (He et al., 2018; Vanlandewijck et al., 2018). Additionally, changes in the polymerization status of cytoskeletal F-actin and α-SMA were proposed to regulate the stiffness and contractility of mid-capillary pericytes (Kureli et al., 2020). Future studies are still required to decipher this ongoing key issue.

Our results suggest that uptake of TO-PRO-3 is mediated through an yet unidentified transporter expressed by brain pericytes, namely, (a) TO-PRO-3 does not permeate membranes (Suzuki et al., 2007) and thus requires a transport system to enter into cells; (b) TO-PRO-3 concentrated into pericytes, and (c) dynamics of dye uptake displayed maximal capacity. Uptake saturation might have reflected the unavailability of additional transporters to carry more dye (Berne and Levy, 2008; Albert et al., 2002). The transporter-mediated transfer of TO-PRO-3 through the pericyte membrane might be passive (facilitated diffusion) or active depending on the sign of the net driving force generated by the electrochemical gradient. Our findings highly suggested that TO-PRO-3 incorporation into brain pericytes is an actively mediated mechanism. First, TO-PRO-3 significantly accumulated into pericytes to a higher concentration as compared to other cells/extracellular solution; second, dye uptake showed high dependence on the temperature (Q10~5.02), and third, a diffusion-based entry of TO-PRO-3 into pericytes through Panx1 channels or Cxs hemichannels was ruled out through pharmacological tools. Besides, hippocampal pericytes from global knock-out mice for Pannexin1 (Panx1$^{-/-}$) were also strongly labeled by TO-PRO-3 (data not shown). That activity of Panx1 channels was dispensable for TO-PRO-3 influx was not consistent with previous studies reported in Jurkat cells where uptake of TO-PRO-3 is Panx1 dependent (Chekeni et al., 2010; Chiu et al., 2017; Good et al., 2018; Poon et al., 2014). If connexons/pannexons eventually admitted a TO-PRO-3 influx, their contribution was negligible as compared to the active transport. Interestingly, previous studies already postulated that

living pericytes can incorporate the large-molecular weight fluorescent probes dextran-conjugated fluorescent calcium indicator Calcium Green I (Hirase et al., 2004), Fluoro-Gold (Edwards et al., 2013) and NeuroTrace 500/525 (Damisah et al., 2017). Accordingly, an active transport mechanism specifically expressed by pericytes was also proposed to underlie NeuroTrace 500/525 entry into living pericytes (Damisah et al., 2017). NeuroTrace 500/525 and TO-PRO-3 Iodide 642/661 share additional properties, that is, both markers stain nucleic acids in fixed sections but they shift their staining profile in living tissue where they selectively label pericytes and both display a similar labeling pattern. At present, whether they also employ the same transporter to enter into pericytes is unknown. The high expression of membrane transporters reported for capillary pericytes (Vanlandewijck et al., 2018) is consistent with the preferential uptake of fluorescent probes by these cells as compared to mural cells from other sections of the vasculature (Berthiaume et al., 2018). Finally, as aforementioned (see results), pericytes from mice aged between P06 and P90 also incorporated TO-PRO-3. These findings suggest that the transport system carrying TO-PRO-3 into pericytes might be present from the early stages of development and maintained during adulthood.

Herein, TO-PRO-3 labeled pericytes of rats and mice neural structures. We do not know whether pericytes from other species or systems (i.e., kidneys, heart) also exhibit selective uptake of TO-PRO-3. Regional differences concerning labeling properties of pericytes have been reported (Edwards et al., 2013). Interestingly, studies on human microvasculature are emerging (Hill et al., 2015; Nortley et al., 2019; Smyth et al., 2018) and using TO-PRO-3 to target pericytes in human tissues would be particularly convenient. Then, future studies might assess if TO-PRO-3 enables pericytes imaging in the human brain and other mammalian tissues.

Ex vivo, labeling pericytes with TO-PRO-3 displayed an outstanding and selective bright fluorescence, which, together with its extensive cellular filling, allowed high-resolution optical images in live and fixed murine sections. Although the TO-PRO-3 fluorescence was highly stable in PFA-fixed slices, we found photobleaching in living time-lapse experiments. Optimization of exposure times during image acquisition could overcome these limitations making TO-PRO-3 appropriate for live imaging (see Figure 5; Lacar et al., 2012). As a DNA-binding dye (Martin et al., 2005), TO-PRO-3 can interfere with cellular processes generating damage. However, herein, we did not find signs of cytotoxicity in long-term experiments (up to 6 hr). Accordingly, the far-red emitting probe TO-PRO-3 Iodide (642/661) displays minimal autofluorescence and phototoxicity (Suseela et al., 2018) compared to fluorophores endowed with other excitation/emission spectra (mostly those excited with UV light). Among these dyes, the above-mentioned dextran-conjugated fluorescent calcium indicator Calcium Green I (506/531) (Hirase et al., 2004), and the neuronal markers Fluoro-Gold (UV) (Edwards et al., 2013) and NeuroTrace (500/525) (Damisah et al., 2017) also label CNS pericytes when administered to living parenchyma. As with TO-PRO-3 labeling, NeuroTrace also yields a remarkable signal-to-noise rapport stain in hippocampal slices. However, as opposed to NeuroTrace which diffuses out of pericytes during immunostaining procedures (Damisah et al., 2017), the TO-PRO-3 mark could bear antibody labeling; this behavior of TO-PRO-3 was similar to Fluoro-Gold, whose compatibility with immunofluorescence has been reported (Edwards et al., 2013). Importantly, TO-PRO-3 displays exclusive emission at 633 excitation in the far-red channel avoiding interference with other fluorescence channels (Bink et al., 2001). This represents a benefit over probes with wider emission profiles and favors its use during multi-labeling, especially in association with widespread used FITC-conjugated probes or green fluorescent protein (GFP) reporters.

5 | CONCLUSIONS

We show here that low concentrations of TO-PRO-3 Iodide (642/661) are selectively taken up by ex vivo living pericytes from the neurovascular unit through an active transporter-mediated process; as a result, pericytes become brightly stained. In addition to the good stability and high signal-to-background ratio exhibited by the TO-PRO-3-fluorescence, the labeling procedure is rapid, non-toxic, and affordable and shows great reproducibility making it a convenient method to trace cerebral pericytes. On top of that, this dye fluoresces in the far-red region of the spectrum well separated from the green and red fluorophores, making it suitable for multiple labeling in fluorescence microscopy. Importantly, tracking TO-PRO-3-marked pericytes circumvents the need for genetically engineered mice or immunohistochemical counter-staining and thus, it can be easily employed in transgenic murine models.

In summary, we conclude that TO-PRO-3-labeling provides a specific and reliable tool to study pericytes at the neurovascular interface. Futures studies are required to determine whether this dye also recognizes pericytes from other organs or species including human tissues.

ACKNOWLEDGEMENTS

The authors thank Drs. Patricia Cassina and Patricia Lagos for providing us with, GFAP and secondary antibodies respectively, Dr. Gustavo Brum for scientific advice and Luis Vitureira, Elbio Agote* (Departamento de Fisiología), Unidad de Reactivos para Biomodelos de Experimentación (URBE), FUNDACIBA and Unidad de Microscopía Confocal, from Facultad de Medicina - Universidad de la República Oriental del Uruguay, for technical assistance. * deceased on February 25th, 2016.

CONFLICT OF INTEREST

No conflict of interest declared.

ORCID

Verónica Abudara https://orcid.org/0000-0003-0703-306X

REFERENCES

Abbott, N. J., Patabendige, A. A., Dolman, D. E., Yusof, S. R., & Begley, D. J. (2010). Structure and function of the blood-brain barrier. *Neurobiology of Diseases*, *37*(1), 13–25.

Abudara, V., Roux, L., Dallérac, G., Matias, I., Dulong, J., Mothet, J. P., Rouach, N., & Giaume, C. (2015). Activated microglia impairs neuroglial interaction by opening Cx43 hemichannels in hippocampal astrocytes. *Glia*, *63*(5), 795–811.

Alarcón-Martínez, L., Yilmaz-Ozcan, S., Yemisci, M., Schallek, J., Kılıç, K., Can, A., Di Polo, A., & Dalkara, T. (2018). Capillary pericytes express α-smooth muscle actin, which requires prevention of filamentous-actin depolymerization for detection. *Elife.*, *7*, pii: e34861.

Alberts, B., Johnson, A., Lewis, J., Raff, M., Roberts, K., & Walter, P. (2002). *Molecular Biology of the Cell*, 4th ed. : Garland Science. Retrieved from: https://www.ncbi.nlm.nih.gov/books/NBK21054/.

Armulik, A., Genové, G., Mäe, M., Nisancioglu, M. H., Wallgard, E., Niaudet, C., He, L., Norlin, J., Lindblom, P., Strittmatter, K., Johansson, B. R., & Betsholtz, C. (2010). Pericytes regulate the blood-brain barrier. *Nature*. *468*(7323):557–561.

Attwell, D., Mishra, A., Hall, C., O'Farrell, F., & Dalkara, T. (2016). What is a pericyte? *Journal of Cerebral Blood Flow and Metabolism*, *36*, 451–455. https://doi.org/10.1177/0271678X15610340

Bandopadhyay, R., Orte, C., Lawrenson, J. G., Reid, A. R., De Silva, S., & Allt, G. (2001). Contractile proteins in pericytes atthe blood-brain and blood-retinal barriers. *Journal of Neurocytology*, *30*(1), 35–44.

Berne, R. M., Koeppen, B. M., Stanton, B. A. (2008). *Berne & levy physiology*. Mosby Elsevier.

Berthiaume, A. A., Hartmann, D. A., Majesky, M. W., Bhat, N. R., & Shih, A. Y. (2018). Pericyte structural remodeling in cerebrovascular health and homeostasis. *Frontiers in Aging Neuroscience*, *10*, 210.

Bink, K., Walch, A., Feuchtinger, A., Eisenmann, H., Hutzler, P., Höfler, H., & Werner, M. (2001). TO-PRO-3 is an optimal fluorescent dye for nuclear counter-staining in dual-colour FISH on paraffin sections. *Histochemistry and Cell Biology*, *115*(4), 293–299. https://doi.org/10.1007/s004180100254

Bondjers, C., He, L., Takemoto, M., Norlin, J., Asker, N., Hellström, M., Lindahl, P., & Betsholtz, C. (2006). Microarray analysis of blood microvessels from PDGF-B and PDGF-Rbeta mutant mice identifies novel markers for brain pericytes. *The FASEB Journal*, *20*(10), 1703–1705.

Chasseigneaux, S., Moraca, Y., Cochois-Guégan, V., Boulay, A. C., Gilbert, A., Le Crom, S., Blugeon, C., Firmo, C., Cisternino, S., Laplanche, J. L., Curis, E., Declèves, X., & Saubaméa, B. (2018). Isolation and differential transcriptome of vascular smooth muscle cells and mid-capillary pericytes from the rat brain. *Scientific Reports*, *8*(1), 12272.

Chekeni, F. B., Elliott, M. R., Sandilos, J. K., Walk, S. F., Kinchen, J. M., Lazarowski, E. R., Armstrong, A. J., Penuela, S., Laird, D. W., Salvesen, G. S., Isakson, B. E., Bayliss, D. A., & Ravichandran, K. S. (2010). Pannexin 1 channels mediate 'find-me' signal release and membrane permeability during apoptosis. *Nature*, *467*(7317), 863–867.

Chiu, Y. H., Jin, X., Medina, C. B., Leonhardt, S. A., Kiessling, V., Bennett, B. C., Shu, S., Tamm, L. K., Yeager, M., Ravichandran, K. S., & Bayliss, D. A. (2017). A quantized mechanism for activation of pannexin channels. *Nature Communications*, *8*, 14324.

Damisah, E. C., Hill, R. A., Tong, L., Murray, K. N., & Grutzendler, J. (2017). A fluoro-Nissl dye identifies pericytes as distinct vascular mural cells during in vivo brain imaging. *Nature Neuroscience*, *20*(7), 1023–1032.

Daneman, R., Zhou, L., Kebede, A. A., & Barres, B. A. (2010). Pericytes are required for blood-brain barrier integrity during embryogenesis. *Nature*, *468*(7323), 562–566.

de Mazière, A. M., Hage, W. J., & Ubbels, G. A. (1996). A method for staining of cell nuclei in Xenopus laevis embryos with cyanine dyes for whole-mount confocal laser scanning microscopy. *Journal of Histochemistry and Cytochemistry*, *44*, 399–402.

Edwards, I. J., Singh, M., Morris, S., Osborne, L., Le Ruez, T., Fuad, M., Deuchars, S. A., & Deuchars, J. (2013). A simple method to fluorescently label pericytes in the CNS and skeletal muscle. *Microvascular Research*, *89*, 164–168.

Eger, E. I. 2nd. (2004). Characteristics of anesthetic agents used for induction and maintenance of general anesthesia. *American Journal of Health-System Pharmacy*; *61*(4):S3–S10.

Ehler, E., Karlhuber, G., Bauer, H. C., & Draeger, A. (1995). Heterogeneity of smooth muscle-associated proteins in mammalian brain microvasculature. *Cell and Tissue Research*, *279*(2), 393–403.

Fernández-Klett, F., Offenhauser, N., Dirnagl, U., Priller, J., & Lindauer, U. (2010). Pericytes in capillaries are contractile in vivo, but arterioles mediate functional hyperemia in the mouse brain. *Proceedings of the National Academy of Sciences of the United States of America*, *107*(51), 22290–22295.

Garré, J. M., Retamal, M. A., Cassina, P., Barbeito, L., Bukauskas, F. F., Sáez, J. C., Bennett, M. V., & Abudara, V. (2010). FGF-1 induces ATP release from spinal astrocytes in culture and opens pannexin and connexin hemichannels. *Proceedings of the National Academy of Sciences of the United States of America*, *107*(52), 22659–22664.

Good, M. E., Chiu, Y. H., Poon, I. K. H., Medina, C. B., Butcher, J. T., Mendu, S. K., DeLalio, L. J., Lohman, A. W., Leitinger, N., Barrett, E., Lorenz, U. M., Desai, B. N., Jaffe, I. Z., Bayliss, D. A., Isakson, B. E., & Ravichandran, K. S. (2018). Pannexin 1 channels as an unexpected new target of the anti-hypertensive drug spironolactone. *Circulation Research*, *122*(4), 606–615.

Grant, R. I., Hartmann, D. A., Underly, R. G., Berthiaume, A. A., Bhat, N. R., & Shih, A. Y. (2019). Organizational hierarchy and structural diversity of microvascular pericytes in adult mouse cortex. *Journal of Cerebral Blood Flow and Metabolism*, *39*(3), 411–425.

Grutzendler, J., & Nedergaard, M. (2019). Cellular control of brain capillary blood flow: Vivo imaging veritas. *Trends Neuroscience*, *42*(8), 528–536.

Hall, C. N., Reynell, C., Gesslein, B., Hamilton, N. B., Mishra, A., Sutherland, B. A., O'Farrell, F. M., Buchan, A. M., Lauritzen, M., & Attwell, D. (2014). Capillary pericytes regulate cerebral blood flow in health and disease. *Nature*, *508*(7494), 55–60.

Hamilton, N. B., Attwell, D., & Hall, C. N. (2010). Pericyte-mediated regulation of capillary diameter: A component of neurovascular coupling in health and disease. *Frontiers in Neuroenergetics*, *2*, pii: 5.

Hartmann, D. A., Berthiaume, A. –A., Grant, R. I., & Harrill, S. A., Noonan, T., Costello, J., Tieu, T., McDowell, K., Faino, A., Kelly, A., Shih, A. Y. (2020). Brain capillary pericytes exert a substantial but slow influence on blood flow. *BioRxiv* [Preprint]. https://doi.org/10.1101/2020.03.26.008763

Hartmann, D. A., Underly, R. G., Watson, A. N., & Shih, A. Y. (2015a). A murine toolbox for imaging the neurovascular unit. *Microcirculation*, *22*(3), 168–182.

Hartmann, D. A., Underly, R. G., Grant, R. I., Watson, A. N., Lindner, V., & Shih, A. Y. (2015b). Pericyte structure and distribution inthe cerebral cortex revealed by highresolution imaging of transgenic mice. *Neurophotonics*, *2*(4), 041402.

He, L., Vanlandewijck, M., Mäe, M. A., Andrae, J., Ando, K., Del Gaudio, F., Nahar, K., Lebouvier, T., Laviña, B., Gouveia, L., Sun, Y., Raschperger, E., Segerstolpe, Å., Liu, J., Gustafsson, S., Räsänen, M., Zarb, Y., Mochizuki, N., Keller, A., … Betsholtz, C. (2018). Single-cell RNA sequencing of mouse brain and lung vascular and vessel-associated cell types. *Science Data*, *5*, 180160.

He, L., Vanlandewijck, M., Raschperger, E., Andaloussi Mäe, M., Jung, B., Lebouvier, T., Ando, K., Hofmann, J., Keller, A., & Betsholtz, C. (2016). Analysis of the brain mural cell transcriptome. *Scientific Reports*, *6*, 35108.

Hill, R. A., Tong, L., Yuan, P., Murikinati, S., Gupta, S., & Grutzendler, J. (2015). Regional blood flow in the normal and ischemic brain is controlled by arteriolar smooth muscle cell contractility and not by capillary pericytes. *Neuron*, *87*(1), 95–110.

Hirase, H., Creso, J., Singleton, M., Barthó, P., & Buzsáki, G. (2004). Two-photon imaging of brain pericytes in vivo using dextran-conjugated dyes. *Glia*, *46*(1), 95–100.

Holzinger, A. (2009). Jasplakinolide: An actin-specific reagent that promotes actin polymerization.Methods. *Molecular Biology*, *586*, 71–87.

Isasi, E., Korte, N., Abudara, V., Attwell, D., & Olivera-Bravo, S. (2019). Glutaric acid affects pericyte contractility and migration: Possible implications for GA-I pathogenesis. *Molecular Neurobiology*, *56*(11), 7694–7707.

Ivanova, E., Corona, C., Eleftheriou, C. G., Bianchimano, P., & Sagdullaev, B. T. Retina-specific targeting of pericytes reveals structural diversity and enables control of capillary blood flow. *BioRxiv* [Preprint]. https://doi.org/10.1101/2020.05.29.124586

Ivanova, E., Toychiev, A. H., Yee, C. W., & Sagdullaev, B. T. (2013). Optimized protocol for retinal wholemount preparation for imaging and immunohistochemistry. *Journal of Visualized Experiments: Jove*, *82*, e51018.

Jung, B., Arnold, T. D., Raschperger, E., Gaengel, K., & Betsholtz, C. (2018). Visualization of vascular mural cells in developing brain using genetically labeled transgenic reporter mice. *Journal of Cerebral Blood Flow & Metabolism*, *38*(3), 456–468.

Kawamura, H., Sugiyama, T., Wu, D. M., Kobayashi, M., Yamanishi, S., Katsumura, K., & Puro, D. G. (2003). ATP: A vasoactive signal in the pericyte-containing microvasculature of the rat retina. *Journal of Physiology*, *551*(Pt 3), 787–799.

Kisler, K., Nelson, A. R., Montagne, A., & Zlokovic, B. V. (2017b). Cerebral blood flow regulation and neurovascular dysfunction in Alzheimer disease. *Nature Reviews Neuroscience*, *18*(7), 419–434. https://doi.org/10.1038/nrn.2017.48

Kisler, K., Nelson, A. R., Rege, S. V., Ramanathan, A., Wang, Y., Ahuja, A., Lazic, D., Tsai, P. S., Zhao, Z., Zhou, Y., Boas, D. A., Sakadžić, S., & Zlokovic, B. V. (2017a). Pericyte degeneration leads to neurovascular uncoupling and limits oxygen supply to brain. *Nature Neuroscience*, *20*(3), 406–416. https://doi.org/10.1038/nn.4489

Kisler, K., Nikolakopoulou, A. M., Sweeney, M. D., Lazic, D., Zhao, Z., & Zlokovic, B. V. (2020). Acute ablation of cortical pericytes leads to rapid neurovascular uncoupling. *Frontiers in Cellular Neuroscience*, *14*, 27.

Kureli, G., Yilmaz-Ozcan, S., Erdener, S. E., Donmez-Demir, B., Yemisci, M., Karatas, H., & Dalkara, T. (2020). F-actin polymerization contributes to pericyte contractility in retinal capillaries. *Experimental Neurology*, *332*, 113392.

Lacar, B., Herman, P., Platel, J. C., Kubera, C., Hyder, F., & Bordey, A. (2012). Neural progenitor cells regulate capillary blood flow in the postnatal subventricular zone. *Journal of Neuroscience*, *32*(46):16435–16448.

Laitinen, L. (1987). Griffonia simplicifolia lectins bind specifically to endothelial cells and some epithelial cells in mouse tissues. *Histochem Journal*, *19*(4):225–234.

Le Beux, Y. J., & Willemot, J. (1978). Actin- and myosin-like filaments in rat brain pericytes. *Anatomical Record*, *190*(4), 811–826.

Lindahl, P., Johansson, B. R., Levéen, P., & Betsholtz, C. (1997). Pericyte loss and microaneurysm formation in PDGF-B-deficient mice. *Science*, *277*(5323), 242–245.

Ma, W., Hui, H., Pelegrin, P., & Surprenant, A. (2009). Pharmacological characterization of pannexin-1 currents expressed in mammalian cells. *Journal of Pharmacology and Experimental Therapeutics*, *328*(2):409–418.

Martin, R. M., Leonhardt, H., & Cardoso, M. C. (2005). DNA labeling in living cells. *Cytometry A*, *67*(1), 45–52.

Mathiisen, T. M., Lehre, K. P., Danbolt, N. C., & Ottersen, O. P. (2010). The perivascular astroglial sheath provides a complete covering of the brain microvessels: An electron microscopic 3D reconstruction. *Glia*, *58*(9), 1094–1103.

Mishra, A., O'Farrell, F. M., Reynell, C., Hamilton, N. B., Hall, C. N., & Attwell, D. (2014). Imaging pericytes and capillary diameter in brain slices and isolated retinae. *Nature Protocols*, *9*(2), 323–336.

Mishra, A., Reynolds, J. P., Chen, Y., Gourine, A. V., Rusakov, D. A., & Attwell, D. (2016). Astrocytes mediate neurovascular signaling to capillary pericytes but not to arterioles. *Nature Neuroscience*, *19*(12), 1619–1627.

Montagne, A., Barnes, S. R., Sweeney, M. D., Halliday, M. R., Sagare, A. P., Zhao, Z., Toga, A. W., Jacobs, R. E., Liu, C. Y., Amezcua, L., Harrington, M. G., Chui, H. C., Law, M., & Zlokovic, B. V. (2015). Blood-brain barrier breakdown in the aging human hippocampus. *Neuron*, *85*(2), 296–302.

Montagne, A., Nation, D. A., Sagare, A. P., Barisano, G., Sweeney, M. D., Chakhoyan, A., Pachicano, M., Joe, E., Nelson, A. R., D'Orazio, L. M., Buennagel, D. P., Harrington, M. G., Benzinger, T. L. S., Fagan, A. M., Ringman, J. M., Schneider, L. S., Morris, J. C., Reiman, E. M., Caselli, R. J., … Zlokovic, B. V. (2020). APOE4 leads to blood-brain barrier dysfunction predicting cognitive decline. *Nature*, *581*(7806), 71–76.

Montagne, A., Nikolakopoulou, A. M., Zhao, Z., Sagare, A. P., Si, G., Lazic, D., Barnes, S. R., Daianu, M., Ramanathan, A., Go, A., Lawson, E. J., Wang, Y., Mack, W. J., Thompson, P. M., Schneider, J. A., Varkey, J., Langen, R., Mullins, E., Jacobs, R. E., & Zlokovic, B. V. (2018). Pericyte degeneration causes white matter dysfunction in the mouse central nervous system. *Nature Medicine*, *24*(3), 326–337.

Nation, D. A., Sweeney, M. D., Montagne, A., Sagare, A. P., D'Orazio, L. M., Pachicano, M., Sepehrband, F., Nelson, A. R., Buennagel, D. P., Harrington, M. G., Benzinger, T. L. S., Fagan, A. M., Ringman, J. M., Schneider, L. S., Morris, J. C., Chui, H. C., Law, M., Toga, A. W., & Zlokovic, B. V. (2019). Blood-brain barrier breakdown is an early biomarker of human cognitive dysfunction. *Nature Medicine*, *25*(2), 270–276.

Nehls, V., & Drenckhahn, D. (1991). Heterogeneity of microvascular pericytes for smooth muscle type alpha-actin. *Journal of Cell Biology*, *113*(1), 147–154.

Nelson, A. R., Sagare, M. A., Wang, Y., Kisler, K., Zhao, Z., & Zlokovic, B. V. (2020). Channelrhodopsin excitation contracts brain pericytes and reduces blood flow in the aging mouse brain *in vivo*. *Frontiers in Aging Neuroscience*, *12*, 108.

Nikolakopoulou, A. M., Montagne, A., Kisler, K., Dai, Z., Wang, Y., Huuskonen, M. T., Sagare, A. P., Lazic, D., Sweeney, M. D., Kong, P., Wang, M., Owens, N. C., Lawson, E. J., Xie, X., Zhao, Z., & Zlokovic, B. V. (2019). Pericyte loss leads to circulatory failure and pleiotrophin depletion causing neuron loss. *Nature Neuroscience*, *22*(7), 1089–1098.

Nishiyama, A., Komitova, M., Suzuki, R., & Zhu, X. (2009). Polydendrocytes (NG2 cells): Multifunctional cells with lineage plasticity.Nat. *Reviews in the Neurosciences*, *10*(1):9–22.

Nortley, R., Korte, N., Izquierdo, P., Hirunpattarasilp, C., Mishra, A., Jaunmuktane, Z., Kyrargyri, V., Pfeiffer, T., Khennouf, L., Madry, C., Gong, H., Richard-Loendt, A., Huang, W., Saito, T., Saido, T. C., Brandner, S., Sethi, H., & Attwell, D. (2019). Amyloid β oligomers constrict human capillaries in Alzheimer's disease via signaling to pericytes. *Science*, *365*(6450), pii: eaav9518.

Ozerdem, U., Grako, K. A., Dahlin-Huppe, K., Monosov, E., & Stallcup, W. B. (2001). NG2 proteoglycan is expressed exclusively by mural cells during vascular morphogenesis. *Developmental Dynamics*, *222*(2), 218–227.

Pelegrin, P., & Surprenant, A. (2006). Pannexin-1 mediates large pore formation and interleukin-1beta release by the ATP-gated P2X7 receptor. *EMBO Journal*, *25*, 5071–5082.

Peppiatt, C. M., Howarth, C., Mobbs, P., & Attwell, D. (2006). Bidirectional control of CNS capillary diameter by pericytes. *Nature*, *443*(7112), 700–704.

Peters, B. P., & Goldstein, I. J. (1979). The use of fluorescein-conjugated Bandeiraea simplicifolia B4-isolectin as a histochemical reagent for the detection of alpha-D-galactopyranosyl groups. Their occurrence in basement membranes. *Experimental Cell Research*, *120*(2), 321–334.

Poon, I. K., Chiu, Y. H., Armstrong, A. J., Kinchen, J. M., Juncadella, I. J., Bayliss, D. A., & Ravichandran, K. S. (2014). Unexpected link between

an antibiotic, pannexin channels and apoptosis. *Nature*, *507*(7492), 329–334.

Rouget, C. (1873). Mémoire sur le développement, la structure et les propriétés physiologiques des capillaires sanguins et lymphatiques. *Arch Physiol Norm Path*, *5*, 603–663.

Sagare, A. P., Bell, R. D., Zhao, Z., Ma, Q., Winkler, E. A., Ramanathan, A., & Zlokovic, B. V. (2013). Pericyte loss influences Alzheimer like neurodegeneration in mice. *Nature Communications*, *4*, 2932.

Smyth, L. C. D., Rustenhoven, J., Scotter, E. L., Schweder, P., Faull, R. L. M., Park, T. I. H., & Dragunow, M. (2018). Markers for human brain pericytes and smooth muscle cells. *Journal of Chemical Neuroanatomy*, *92*, 48–60.

Suseela, Y. V., Narayanaswamy, N., & Pratihar, S. (2018). Far-red fluorescent probes for canonical and non-canonical nucleic acid structures: Current progress and future implications. *Chemical Society Reviews*, *47*(3), 1098–1131.

Suzuki, T., Fujikura, K., Higashiyama, T., & Takata, K. (1997). DNA staining for fluorescence and laser confocal microscopy. *Journal of Histochemistry and Cytochemistry*, *45*(1), 49–53.

Suzuki, T., Matsuzaki, T., Hagiwara, H., Aoki, T., & Takata, K. (2007). Recent advances in fluorescent labeling techniques for fluorescence microscopy. *Acta Histochemica Et Cytochemica*, *40*(5), 131–137.

Van Hooijdonk, C. A., Glade, C. P., & Van Erp, P. E. (1994). TO-PRO-3 iodide: A novel HeNe laser-excitable DNA stain asan alternative for propidium iodide in multiparameter flow cytometry. *Cytometry*, *17*(2), 185–189.

Vanlandewijck, M., He, L., Mäe, M. A., Andrae, J., Ando, K., Del Gaudio, F., Nahar, K., Lebouvier, T., Laviña, B., Gouveia, L., Sun, Y., Raschperger, E., Räsänen, M., Zarb, Y., Mochizuki, N., Keller, A., Lendahl, U., & Betsholtz, C. (2018). A molecular atlas of cell types and zonation in the brain vasculature. *Nature*, *554*(7693), 475–480.

Wei, H. S., Kang, H., Rasheed, I. D., Zhou, S., Lou, N., Gershteyn, A., McConnell, E. D., Wang, Y., Richardson, K. E., Palmer, A. F., Xu, C., Wan, J., & Nedergaard, M. (2016). Erythrocytes are oxygen-sensing regulators of the cerebral microcirculation. *Neuron*, *91*(4), 851–862. https://doi.org/10.1016/j.neuron.2016.07.016

Yardeni, T., Eckhaus, M., Morris, H. D., Huizing, M., & Hoogstraten-Miller, S. (2011). Retro-orbital injections in mice. *Lab Anim (NY).*, *40*(5), 155–160.

Yemisci, M., Gursoy-Ozdemir, Y., Vural, A., Can, A., Topalkara, K., & Dalkara, T. (2009). Pericyte contraction induced by oxidative-nitrative stress impairs capillary reflow despite successful opening of an occluded cerebral artery. *Nature Medicine*, *15*(9), 1031–1037.

SUPPORTING INFORMATION

Additional supporting information may be found online in the Supporting Information section.

How to cite this article: Mai-Morente SP, Marset VM, Blanco F, Isasi EE, Abudara V. A nuclear fluorescent dye identifies pericytes at the neurovascular unit. *J Neurochem* 2020;00:1–15. https://doi.org/10.1111/jnc.15193